Design of experiments: optimisation of an ITO sputtering recipe

Florent-Valéry Coen
Damien Maillard
Matthias Neuenschwander

Introduction

Multimodal stimulation of the nervous system

The human nervous system is among the most complex biological structures on this planet. The brain alone is composed of tens of billions of neurons (Pakkenberg and Gundersen, 1988) and is solely responsible for coordinating the behavioral responses to the sensory inputs of the body. As a result, it became apparent early on in the field of neuroscience, that the ability to selectively interrogate a population of neurons would be the key element in understanding and controlling the nervous system (Crick, 1979).

Over the years, researchers have devised numerous methods to interact with neural tissues such as electrical and chemical stimuli and, more recently, through mechanical and optical means. Each of these methods has its limitation, particularly when it comes to selectivity. In that regard, neuroscientist typically discriminate between three types of selectivity (figure):

1. Spacial selectivity, which refers to the ability to stimulate a specific volume of tissue.
2. Structural selectivity which describes the capability to stimulate specific structure within a neuron, such as neuronal somata or fibers of passage.
3. Cell-type selectivity relates to the ability to discriminate between neuronal types, a particularly interesting proposition as it would allow to activate only a specific function within a complex network of neurons.

At the LSBI we aim to fabricate so-called multimodal devices, that is, neural implants capable of stimulating the nervous system through multiple methods, in a simultaneous and collocal fashion. We thus hope to improve the selectivity of the combined stimulation and, consequently, to improve our ability to study and control nervous tissues. In particular, we are interested in designing an implant that would incorporate electrical and optical capabilities at the exact same location. In our current prototype, such a feature is realized by placing microLEDs behind transparent electrodes.

The selection of the material used for the electrodes is critical as we thrive to maximize both the amount of electrical charges and light injected in the tissue. At the current stage of research, we use a ceramic called Indium Tin Oxide. This material was recently introduced in the cleanroom facility of Campus Biotech (Geneva) and as such, its deposition method has yet to be tuned for optimal performances of the final film. With this project, we aimed at addressing this shortcoming by optimizing the deposition parameters of the machine used to form Indium Tin Oxide.

Indium Tin Oxide

Indium-tin-oxide (ITO) has long been the center of growing attention because of its exciting and attractive properties. Its relatively low electrical resistivity (2-4e-4 [Ω cm]) combined with high optical transmittance (>85%) make it a material of choice in both research institutes and industry (Kim et al., 1999).

For example, ITO films have long found applications in solar cells. As early as 1978, Cheek et al. showed the fabrication and characterization of ITO/polycrystalline silicon solar cells using ion-beam sputtering techniques (Cheek et al., 1978). A few years later, Saim and Campbell presented a fabrication technique based on conventional thick film print-

ing methods. The ITO film was used here not only as a conducting surface layer, but also as an anti-reflective coating (Saim and Campbell, 1987). More recently, ITO has also been used as a semiconductor material in solar cells (Yu et al., 2016).

Galstian et al. developed a electrically tunable liquid crystal autofocus lens. To achieve electrical contact while keeping optical transmittance at its best, the lens needs to be coated with transparent electrodes. Indium-tin-oxide is thus the ideal material for this application (Galstian et al., 2017).

Since the 1990s, ITO thin films were also found in liquid-crystal displays (Ishibashi et al., 1990; Sawada et al., 2001), where they are used to form the transparent electrodes necessary to the realization of high resolution flat panel. This is precisely the time of use case we want to mimic.

Methods

Deposition

The ITO films were formed using a commercial sputtering system (Alliance Concept AC450). Sputtering is a deposition technique in which a target material is bombarded with the highly energetic ions from a plasma, leading to the ejection of atoms toward a sample. On the AC450, the quality of the resulting film can be controlled via six parameters (Table 1):

1. The electrical field applied between the target material and the chuck holding the sample. The strength and nature of the field are controlled by the power values of its DC and RF components.
2. The base pressure, i.e. the quality of the vacuum inside the chamber at the start of the sputtering phase.
3. The temperature of the chuck holding the sample.
4. The distance between the target and the chuck holding the sample during the deposition.
5. The argon flow fed inside the chamber and used to create and sustain the plasma.

	1: Argon	2: Oxygen	3: Temperature	4: DC Power	5: P
	sccm	*sccm*	*degC*	*W*	*m*
1	36	2.4	300	180	9
-1	24	1.6	20	120	6

Table 1: Experiment parameters: maximum and minimum values for all considered parameters.

6. The oxygen flow fed inside the chamber. Not only are the oxygen atoms used to generate the plasma, they also contribute to the creation of defect inside the ITO lattice - this is the main mechanism through which ITO is made conductive.

For this project, we decided to limit our investigation to five parameters by keeping the distance between the target and the chuck constant across all experiments. We also chose to keep the RF component of the electric field null and to only vary the value of the DC power. This last decision was made based on the fact that DC recipes naturally lead to faster deposition rates and thus faster turnaround, a critical consideration during the prototyping phase of a device.

In order to ensure that the quantity of deposited material would be sufficient for the characterization process, we set a target thickness of 100nm. We thus started our investigation by assessing the deposition rate for each set of parameters during a series of calibration runs. To do so, we ran each recipe for 10 minutes, before measuring the resulting film thickness using an atomic force microscope (AFM). Based on these measurements, we were able to estimate each deposition rate, which we then used to compute an appropriate deposition time for the characterization samples.

Film characterization

Resistivity

We assessed the resistivity of our ITO films using a 4-point probe station, namely the KLA-Tencor Prometrix Omnimap RS75, available in the CMi at EPFL. Measurements are performed in the following

way : the tool first contacts 4 aligned electrical probes to the film. Then, a DC current is applied between the 2 outer probes, and the voltage between the 2 inner probes is recorded. We thus obtain the sheet resistance of our sample, following the equation :

$$R_s = \frac{\pi}{ln(2)} \frac{V}{I}$$

The actual resistivity can easily be calculated knowing the thickness of the film :

$$\rho = R_s \cdot t$$

Transmittance

We measured the transmittance of our samples with a spectroscopic transmittometer and turned to the Filmetrics F20 UV in the CMi at EPFL. We performed the measurement over the range from 200nm to 1100nm, and then focused on the value obtained at 460nm (see Fig. 1). This is the wavelength that will result in the opening of the light-sensitive ion channels present in the neurons of the transfected mice used in our experiments.

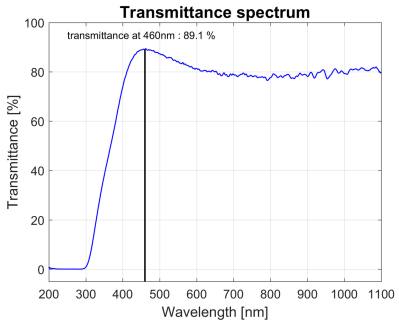

Figure 1: Typical transmittance spectrum and its value at 460nm as measured by the Filmetrics F20 UV in CMi, at EPFL.

Deposition rate

We determined the exact deposition rate with an atomic force microscope (AFM). Before the deposition experiments, we marked the exposed side of the glass samples with a red marker pen. As the marker ink is dissolved in IPA, we could perform a lift-off of ITO at those locations. We then measured the resulting step height between the ITO layer and the glass substrate. Dividing that value by the exact sputtering time yielded a precise value for the deposition rate.

Run	1: Argon	2: Oxygen	3: Temperature	4: DC Po
1	-1	-1	-1	1
2	-1	1	1	-1
3	-1	1	-1	1
4	-1	-1	1	-1
5	1	-1	-1	-1
6	1	1	1	1
7	1	1	-1	-1
8	1	-1	1	1
9	0	0	0	0

Table 2: Experiment matrix: the eight runs of the fractional factorial design were completed with a center point run.

Design of experiment

Assuming the responses of the experiment can be approximated well with a linear model, we opted for a fractional factorial design. For the first round of measurements, we chose to design the experiment such as to minimise the costs. As we have five factors, we used a 2^{5-3} design (Table 2) with the generator (1, 2, 3, 13, 23), yielding 8 measurement runs to perform. We added a null run in order to be able to test the lack-of-fit.

The system is of resolution III, meaning that the main effects are aliased with first order interactions (Table 3). The chuck temperature is the only factor not defining the plasma, we thus expect it to have little interaction with the other factors. In order to limit aliasing on the other factors, we chose the temperature to be factor 3. If required, after analysis of the first round of experiments it is possible to extend the experiment matrix with 8 additional runs and obtain a 2^{5-1} fractional factorial design, allowing de-aliasing of the main effects and the first order interactions.

Contrast	Term	Confounding
Argon	1	34
Oxygen	2	35
Temperature	3	14+25
DC Power	4	13
Pressure	5	23
Interaction	12	45
Interaction	15	25

Table 3: Aliasing: the main effects are confounded with first order interactions.

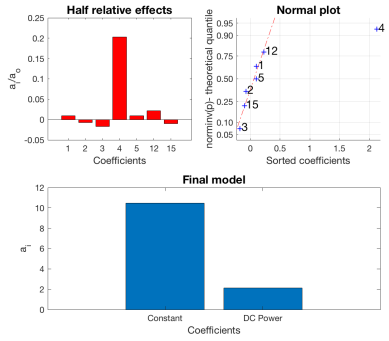

Figure 2: Deposition rate analysis. The relative half effects and the normal distribution show that only the effect of factor 4 (DC power) is significant. The fitted linear regression model (1+x4) is good (p-value is 2.05E-06). There is no lack of fit (p-value of 0.20).

Run	1: Argon *sccm*	2: Oxygen *sccm*	3: Temperature $^{\circ}C$	4: DC Power *W*	5: Pressure *mbar*	Deposition Rate *nm/min*	Resistivity $\Omega \cdot cm$	Transmitta %
1	-1	-1	-1	1	-1	13.1	0.1498	85.3
2	-1	1	1	-1	-1	9.1	0.0006	87.2
3	-1	1	-1	1	1	12.1	0.0017	87.2
4	-1	-1	1	-1	1	7.9	0.0333	86.2
5	1	-1	-1	-1	-1	8.4	0.0034	88.6
6	1	1	1	1	-1	12.3	0.0007	84.9
7	1	1	-1	-1	1	8.7	0.0007	88.9
8	1	-1	1	1	1	12.6	0.0011	87.2
9	0	0	0	0	0	11.0	0.0011	84.0

Table 4: Results of the characterization of the nine experiment runs.

Results

The results from the 9 experimental runs are shown in Table 4.

Deposition rate

The results show that only one factor is significant (Fig. 2). Indeed, increasing the DC power accelerates the deposition rate, while varying all other factors have no significant impact.

Resistivity

Studies showed that sheet resistance sputtered ITO films is proportional to the inverse of temperature and pressure (Yasrebi et al., 2014). It follows that sheet conductance, and thus material conductivity vary linearly with the temperature and pressure. We thus decided to use the conductivity, rather than resistivity as the experiment response. This justifies the use of a linear regression model.

The model (Fig. 3) shows that increasing Argon flow and temperature, as well as decreasing the base pressure will increase the conductivity. However it is important to remember that the temperature effect is aliased with potentially important interactions. Additional experiments can be performed to de-alias the main effects from first order interactions.

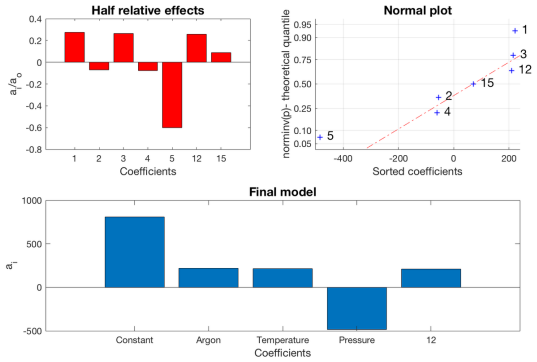

Figure 3: Conductivity analysis. The relative half effects show that Argon flow, temperature and pressure are relevant. There are also some non-negligible interactions. The fitted linear regression model (1+x1+x3+x5+x1:x2) is reasonable(p-value is 3.42E-03).

Transmittance

The transmittance analysis (Fig. 4) does not allow us to quantify the effects of the factors, as their values are within the uncertainty of the data. However we expect the effects to be relatively small compared to the constant: indeed the relative half effects are below the 1% mark.

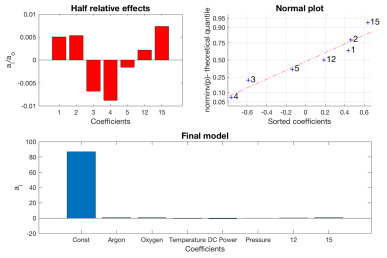

Figure 4: Transmittance analysis. The relative half effects and the normal plot show that we do not have enough information to define which factors have a relevant effect on transmittance. The p-values of all factors except the intercept are far above 5%.

Conclusion

We were able to learn some valuable information about the characteristics of sputtered ITO films. We have determined the dependance of the deposition rate on the sputtering parameters. The transmittance changes only in small amounts within our experiment design space; this indicates that it may not be necessary to consider transmittance as a response for which to optimise the sputtering process. In contrast, the resistivity can change by a couple of orders of magnitude, depending on the parameters. We determined which factors have relevant effects, but also noticed that some interactions are non negligible. As our fractional factorial design does not allow to distinguish between main effect and first order interaction, future work should include a set of additional experiments, carefully chosen in order to de-aliase our results.

References

G. Cheek, N. Inoue, S. Goodnick, A. Genis, C. Wilmsen, and J. B. DuBow. Fabrication and characterization of indium tin oxide (ITO)/polycrystalline silicon solar cells. *Applied Physics Letters*, 33(7): 643–645, oct 1978. doi: 10.1063/1.90448. URL https://doi.org/10.1063%2F1.90448.

F. H. C. Crick. Thinking about the Brain. *Scientific American*, 241(3):219–232, sep 1979. doi: 10.1038/scientificamerican0979-219. URL https://doi.org/10.1038%2Fscientificamerican0979-219.

T. Galstian, O. Sova, K. Asatryan, V. Presniakov, A. Zohrabyan, and M. Evensen. Optical camera with liquid crystal autofocus lens. *Optics Express*, 25(24):29945, nov 2017. doi: 10.1364/oe.25.029945. URL https://doi.org/10.1364%2Foe.25.029945.

S. Ishibashi, Y. Higuchi, Y. Ota, and K. Nakamura. Low resistivity indium–tin oxide transparent conductive films. II. Effect of sputtering voltage on electrical property of films. *Journal of Vacuum Science & Technology A: Vacuum Surfaces, and Films*, 8(3):1403–1406, may 1990. doi: 10.1116/1.576890. URL https://doi.org/10.1116%2F1.576890.

H. Kim, C. M. Gilmore, A. Piqué, J. S. Horwitz, H. Mattoussi, H. Murata, Z. H. Kafafi, and D. B. Chrisey. Electrical optical, and structural properties of indium–tin–oxide thin films for organic light-emitting devices. *Journal of Applied Physics*, 86 (11):6451–6461, dec 1999. doi: 10.1063/1.371708. URL https://doi.org/10.1063%2F1.371708.

B. Pakkenberg and H. J. G. Gundersen. Total number of neurons and glial cells in human brain nuclei estimated by the disector and the fractionator. *Journal of Microscopy*, 150(1):1–20, apr 1988. doi: 10.1111/j.1365-2818.1988.tb04582.x. URL https://doi.org/10.1111%2Fj.1365-2818.1988.tb04582.x.

H.B. Saim and D.S. Campbell. Properties of indium-tin-oxide (ITO)/silicon heterojunction solar cells by thick-film techniques. *Solar Energy Materials*, 15(4):249–260, may 1987. doi: 10.1016/0165-1633(87)90040-2. URL https://doi.org/10.1016%2F0165-1633%2887%2990040-2.

Masato Sawada, Masatoshi Higuchi, Susumu Kondo, and Hiroyasu Saka. Characteristics of Indium-Tin-Oxide/Silver/Indium-Tin-Oxide Sandwich Films and Their Application to Simple-Matrix Liquid-Crystal Displays. *Japanese Journal of Applied Physics*, 40(Part 1 No. 5A):3332–3336, may 2001. doi: 10.1143/jjap.40.3332. URL https://doi.org/10.1143%2Fjjap.40.3332.

Navid Yasrebi, Behrang Bagheri, Payam Yazdanfar, Bizhan Rashidian, and Pezhman Sasanpour. Optimization of Sputtering Parameters for the Deposition of Low Resistivity Indium Tin Oxide Thin Films. *Acta Metallurgica Sinica (English Letters)*, 27(2):324–330, 2014.

Ze Yu, Ishanie R Perera, Torben Daeneke, Satoshi Makuta, Yasuhiro Tachibana, Jacek J Jasieniak, Amaresh Mishra, Peter Bäuerle, Leone Spiccia, and Udo Bach. Indium tin oxide as a semiconductor material in efficient p-type dye-sensitized solar cells. *NPG Asia Materials*, 8(9):e305–e305, sep 2016. doi: 10.1038/am.2016.89. URL https://doi.org/10.1038%2Fam.2016.89.